

Preparation of PVA-KOH-Halloysite Nanotube Alkaline Solid Polymer Electrolyte and its Application in Ni-MH Battery

Lidan Fan², Juan Chen¹, Gang Qin^{2,*}, Libo Wang¹, Xiaoyi Hu¹, Zhongshuo Shen¹

¹ School of Civil Engineering, Henan Polytechnic University, Jiaozuo 454001, China

² School of Materials Science and Engineering, Henan Polytechnic University, Jiaozuo 454001, China

*E-mail: qingang@hpu.edu.cn

Received: 23 January 2017 / Accepted: 14 April 2017 / Published: 12 May 2017

Alkaline solid polymer electrolytes (ASPEs) comprising of poly(vinyl alcohol) (PVA) and KOH with addition of natural halloysites (HNTs) nanotube have been prepared. The ionic conductivity and thermal stability of ASPE were improved by the blending of HNTs. The PVA-KOH-HNTs ASPE with m(PVA): m(KOH)=1.5:1.5 and HNTs=8 wt% exhibited the highest ionic conductivity of $0.071 \text{ S}\cdot\text{cm}^{-1}$ at 30 °C. The microstructures of the PVA-KOH-HNTs ASPEs were measured by FTIR and XRD, and the micro-porous morphology was observed by SEM. The influence of temperature on the ionic conductivity was detected. To investigate the electrochemical properties of the ASPE, a Ni-MH battery with the configuration of hydrogen storage alloy/PVA-KOH-HNTs/Ni(OH)₂ was fabricated. The highest discharge capacity of $223 \text{ mAh}\cdot\text{g}^{-1}$ was obtained.

Keywords: Alkaline polymer electrolyte; Halloysites; Ionic conductivity; Ni-MH battery

1. INTRODUCTION

Research and development of alkaline solid polymer electrolytes (ASPEs) have received attention due to the potential application for rechargeable alkaline batteries and supercapacitors. Compared to conventional alkaline aqueous electrolyte, ASPEs could provide some advantages such as safer design, flame-resistance, shape suitability, easy preparation, soft packaging and better electrochemical stability [1-4]. In the ASPEs, potassium hydroxide (KOH) generally acts as ionic dopant [5], and various polymers like poly(ethylene oxide) [6], poly(vinyl alcohol) (PVA) [7], poly(acrylic acid) [8], polyepichlorohydrin [9] and their blends[10] or copolymers [11] have been used as polymer matrix. Among them, PVA is considered suitable choice because of high dielectric strength, good chemical stability, membrane-forming ability, low cost, dopant-dependent electrical and

optical properties. PVA is a water-soluble and semicrystalline polymer and could readily form gel. PVA is also biocompatible and biodegradable, and is widely used in medical, cosmetic, and packaging materials.

One major limitation of ASPE's applications is their mechanical and electrochemical properties [12]. And several investigations have been carried out such as blending and copolymerization of polymer matrix [13] and doping with nanoparticles. Herein, the addition of nano-scale ceramic fillers to prepare composite alkaline polymer electrolytes has been proved an effective method to improve the ambient temperature conductivity, because of the reinforcing effect, lower glass transition temperature and more amorphous region of matrix. Various nano-scale fillers including TiO_2 [14], ZrO_2 [15], Al_2O_3 [16], SiO_2 [17], Bentonite [18], and glass-fibre [19] have been applied to the ASPEs and the predictive effects were obtained.

Halloysite ($\text{Al}_2\text{Si}_2\text{O}_5(\text{OH})_4 \cdot 2\text{H}_2\text{O}$) nanotubes (HNTs) are a type of natural clay with nanotubular structure formed by rolling layers of tetrahedral sheets of silica as outer surface and octahedral sheets of alumina as lumen surface. Unlike the well-known carbon nanotubes, they are typical natural nanotubes, which are about 500~2000 nm length, 50~100 nm diameter with a mean thickness of 20 nm in the wall of the tube (Figure 1). HNTs can be divided into two types: 7 Å and 10 Å HNTs based on the hydration level [20-22]. Growing attention has been attracted on HNTs during recent years due to their excellent adsorption capacity, mechanical property, biocompatibility, unique surface chemical state and cost-effectiveness [23,24]. Therefore, HNTs are widely used as drug carrier, hydrogen storage, catalyst, nanoreactor, the templates of preparing nanomaterials and so on [25-27]. In particular, HNTs have been demonstrated to be an ideal component for fabricating high-performance polymer nanocomposites [28,29].

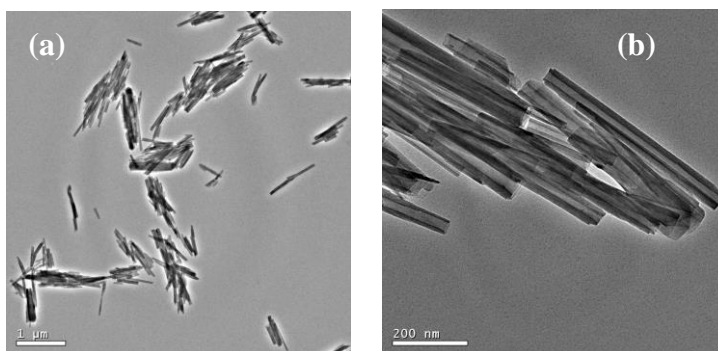


Figure 1. Low (a) and high (b) magnifying TEM photographs of HNTs

Based on the principle of nano composite polymer electrolytes, in this work, we made an attempt to improve the electrochemical and thermal properties of PVA-KOH ASPE through the adding of HNTs. The structure of the composite ASPE was investigated by scan electron microscope (SEM), Fourier transform infrared spectroscopy (FTIR) and X-ray diffraction (XRD), and the important performances such as ionic conductivity, electrochemical stability and thermal stability were measured and the influence factors were discussed. To the best of our knowledge, the usage of HNTs as filler for

ASPE has not been reported previously. In addition, simulated polymer Ni-MH battery with PVA-KOH-HNTs ASPE as electrolytes was assembled and tested.

2. EXPERIMENTAL

2.1 Preparation of PVA-KOH-HNTs ASPE membranes

PVA124 was manufactured by Kuraray Co., Japan, with molecular weight of 105,600 and alcoholysis degree of 99%. HNTs was mined from Henan, China and further treated according to the procedure [30] and dried in a vacuum oven at 80 °C for 12 h. The ASPE was prepared by sol-gel method. PVA (1.5g) and HNTs were mixed with different HNTs concentration (0, 2, 4, 6, 8, 10 wt%) and dissolved in 10 mL deionized water followed by stirring for 1 h at 90 °C. Different quantities of KOH were dissolved in another 10 mL deionized water and stirred for a few minutes. These solutions were mixed together and stirred again for another 2 h. The solutions were poured into different Petri dishes and the ASPE was obtained after drying at room temperature (about 25 °C).

2.2 Preparation of PVA-KOH-HNTs polymer Ni-MH batteries

A hydrogen storage alloy powder (Ni: 55.0±1.0 wt%; Co: 6.1±0.5 wt%; Mn: 4.8±0.5 wt%; Al: 1.9±0.5 wt%) was used as negative electrode material. The homogeneous mixture of 0.15 g alloy powder and 0.75 g carbonyl nickel powder was cold-pressed into a pellet of 10 mm diameter and about 0.5 mm thickness under the pressure of 15 MPa. Positive electrode was commercial sintered Ni(OH)₂/NiOOH electrode (Highstar Group Company, China). The experimental polymer Ni-MH batteries were constructed by sandwiching the PVA-KOH-HNTs ASPE membrane between the hydrogen storage alloys negative electrode and the sintered Ni(OH)₂/NiOOH positive electrode.

2.3 Measurement

FTIR was carried by using a FTIR spectrometer (Shimadzu 2000, Shimadzu Co.) in the range of 400-4000 cm⁻¹. XRD was performed by X-ray diffractometer (D-500, Siemens Ltd.) using Cu K α radiation and operating at 40 kV and 150 mA at wavelength 0.154 nm, 2 θ : 5~90°. The morphologies of HNTs and ASPE membrane were investigated by a TEM H-600 (HITACHI Co.) and a SEM (FESEM, Hitachi S4800), respectively. The membranes were fractured in liquid nitrogen and sputtered with gold, then examined at 10 kV. The TGA (DSC-Q10, TA Company) was tested in the temperature range of room temperature~600 °C with a scanning rate of 10 °C·min⁻¹ under argon atmosphere. The chopped pieces of ASPE were used as samples without predry.

The ionic conductivity and electrochemical stability of the AGPE were determined by an electrochemical workstation (Parstat2273, Princeton Applied Research Company). The electrical conductivity of polymer electrolyte membranes was determined by impedance spectra with frequency range from 100 kHz to 0.1 Hz at an excitation signal of 5 mV. The samples were assembled by

sandwiching the membranes between two stainless steel (SS) blocking electrodes. The electrochemical stability window measurement was performed by cyclic voltammogram for setting a cycle voltage region from -1.5 to +1.5 V at a scan rate of $20 \text{ mV}\cdot\text{s}^{-1}$ by using the same SS|ASPE|SS cell at $30 \text{ }^\circ\text{C}$. The charge-discharge performance of the polymer Ni-MH batteries and the traditional Ni-MH battery was monitored by the Neware (CT-3008) battery test instrument (Neware Technology Co. Ltd., China), and the battery was charged at 10.0 mA for 4 h and discharged at 0.3 mA after 10 min resting.

3. RESULTS AND DISCUSSION

3.1 FTIR

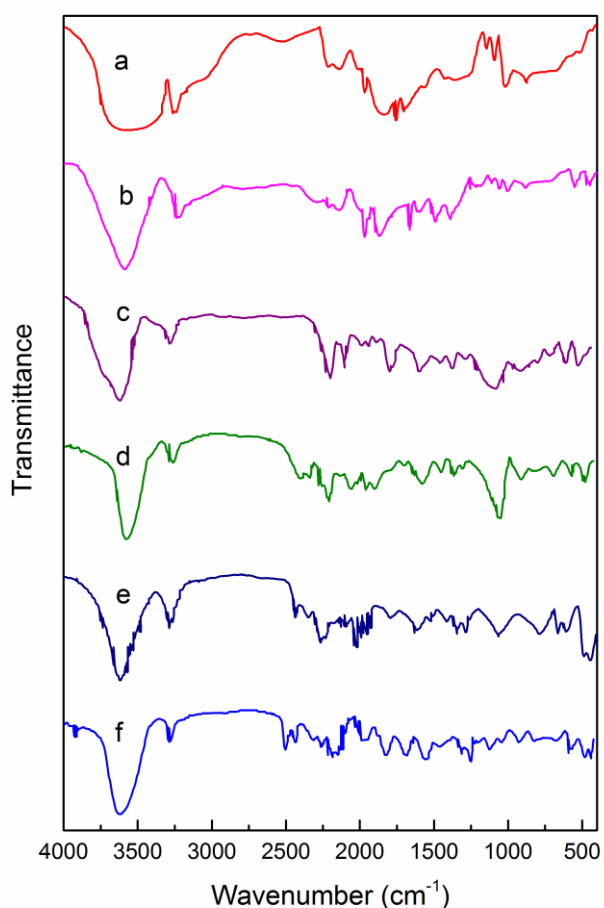


Figure 2. FTIR spectra of PVA-KOH-HNTs ASPEs with different HNTs contents.(m(PVA): m(KOH)=1.5:1.5; a, 0 wt% HNTs; b, 2 wt% HNTs; c, 4 wt% HNTs; d, 6 wt% HNTs; e, 8 wt% HNTs; f, 10 wt% HNTs)

FTIR spectroscopic technique is one of the most effective methods for the investigation of interaction between polymer and the filler. The FTIR spectra of PVA-KOH-HNTs ASPE (m(PVA):

m(KOH)=1.5:1.5) with different HNTs content are illustrated in Figure 2. All of the spectra showed an intense band between 3100 and 3750 cm^{-1} , which was ascribed to the stretching vibration of -OH groups from the bound water. The spectrum 2a displayed typical PVA absorption bands such as the stretching vibration and flexural vibration of -OH group at 3,363 and 1,372 cm^{-1} , respectively. The characteristic absorption peaks at 2,917 and 2,845 cm^{-1} were assigned to the asymmetric and symmetric stretching vibrations of the $-\text{CH}_2$ [31], and at about 1089 and 1451 cm^{-1} for the -C-O group. The band at 1715 cm^{-1} coincided with the carbonyl groups of remanent acetate groups reserving after the preparation of PVA from the hydrolysis of poly(vinyl acetate) [32].

The composites with HNTs were chemically characterized as presented in spectra 5b~f, where the 469 and 533 cm^{-1} bands were likely to be in accord with Si-O-Si and Al-O-Si vibration. While the absorption at 912 cm^{-1} was associated with inner -OH group of HNTs nanotube [33]. The characteristic absorption peak at 1027 cm^{-1} corresponded to the vibrations of the Si-O band, and the strength increased as the HNTs content increasing. The absorbance at 1098 cm^{-1} was related to C-O stretching, which became weaker as a result of the formation of new bonds between PVA and HNTs with the addition of HNTs. Besides, the peak intensities of $-\text{CH}_2$ and $-\text{CH}-$ bands also reduced perhaps on account of the restricted motion of PVA chain in the presence of HNTs. The interaction between PVA matrix and HNTs filler could be proved by such changes and shiftings.

3.2 XRD

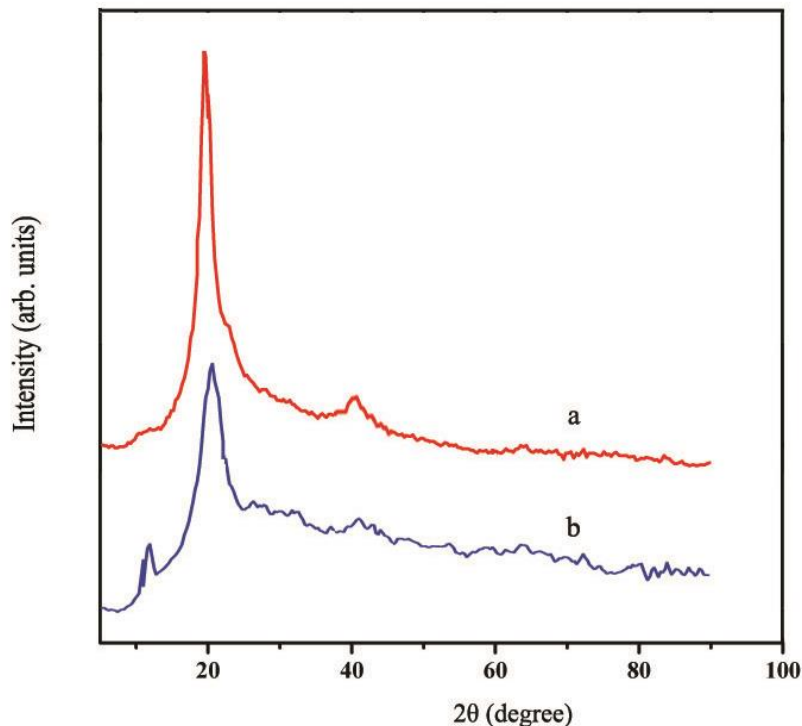


Figure 3. XRD patterns of the PVA-KOH (a) and PVA-KOH-HNTs (b) membranes (m(PVA): m(KOH)=1.5:1.5, HNTs=8 wt%)

The crystallinity of PVA-KOH and PVA-KOH-HNTs (m(PVA): m(KOH)=1.5:1.5, HNTs=8 wt%) ASPE was analyzed by XRD as shown in Figure 3. XRD pattern of PVA-KOH membrane (spectrum 4a) is used as a reference. The diffractogram showed peaks at 19.7° (Fig. 3a) and 20.2° (Fig. 3b) associated with the crystalline plane (101), indicating the semi-crystalline structure of PVA due to the high hydrogen bond of hydroxyl groups. And the semi-crystalline structure was also proved by another peak with low intensity appears at about $2\theta=41^\circ$ [34].

In the case of PVA-KOH-HNTs ASPE, a diffraction peak appeared at $2\theta=12.25^\circ$ that was related to (001) plane. This 2θ value indicated that the d-spacing was 0.73 nm, which implied that the HNTs used in this experiment were the dehydrated 7\AA -HNTs [35]. All of the observed peaks were close to the characteristic data of HNT (JCPDS card No. 29-1487). The characteristic peaks of HNTs were observed in the composites, indicating that the crystalline structure had remained after blending. In the meantime, the intensity of the PVA characteristic peaks weakened with the addition of HNTs because of the inhibition of the crystalline structure.

3.3 Morphology

SEM photograph of the PVA-KOH-HNTs (m(PVA): m(KOH)=1.5:1.5, HNTs=8 wt%) ASPE membrane surface is illustrated in Figure 4 at a magnification of $12,000\times$. The surface morphology of membrane was rough and porous. Many micro pores with dimension of about $0.3\sim 1\ \mu\text{m}$ could be observed on the surface and a three-dimensional network structure maybe formed. Water uptake improved resulting from such structure and more KOH electrolyte would be contained in ASPE membrane, which was beneficial to the ionic conductivity. It was found that there was no phase separation between PVA and HNTs. The composite PVA-KOH-HNTs ASPE was uniform and homogenous when the content of HNTs was 8 wt%.

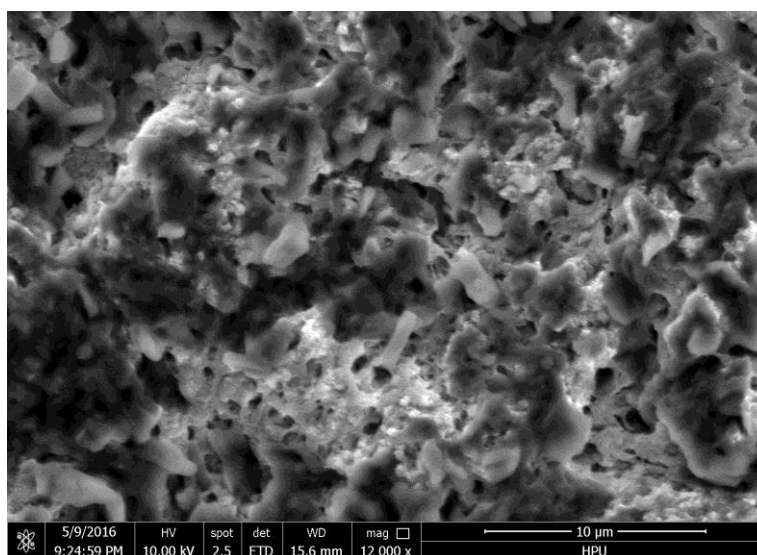


Figure 4. SEM photograph of the PVA-KOH-HNTs ASPE (m(PVA): m(KOH)=1.5:1.5, HNTs=8 wt%)

3.4 Ionic conductivity

To test the ionic conductivity of the PVA-HNTs-KOH membranes, AC impedance experiments were performed on each sample. The influence of the content of HNTs on the conductivity of the composite ASPE ($m(\text{KOH}):m(\text{PVA})=1.5:1.5$) at 30 °C was investigated firstly as exhibited in Figure 5. As expected, all spectra presented a similar trend which showed the typically non-vertical spike for blocking electrodes, i.e., SS|PVA-HNTs-KOH SPE|SS cell. The intercept on the real axis on the high frequency side provided the bulk resistance (R_b) [36], which was used to calculate the electrical conductivity. The R_b was 0.65 Ω for the PVA-KOH ASPE before the doping of HNTs, and it decreased as the content of HNTs increased gradually until the R_b was 0.36 Ω with 8 wt% HNTs, however, it increased again to 0.57 Ω when the HNTs content was 10 wt%.

Taking into account the thickness of the nanocomposite ASPE membranes, the R_b value could be converted into ionic conductivity value (σ) according to equation 1 [37]:

$$\sigma = \frac{L}{R_b A} \text{ (equation 1)}$$

where L is the thickness (cm) of the PVA-HNTs-KOH membrane, A is the area of the blocking electrode (cm^2).

The R_b and σ values of the PVA-HNTs-KOH ASPEs are listed in Table 1, indicating that the conductivity was depended on the HNTs content significantly. It was evident from Table 1 that the R_b values were only in the range of 0.3~0.7 Ω and the σ values were more than 0.03 $\text{S}\cdot\text{cm}^{-1}$. It was observed that the highest σ was 0.071 $\text{S}\cdot\text{cm}^{-1}$ with the corresponding HNTs content was 8 wt%.

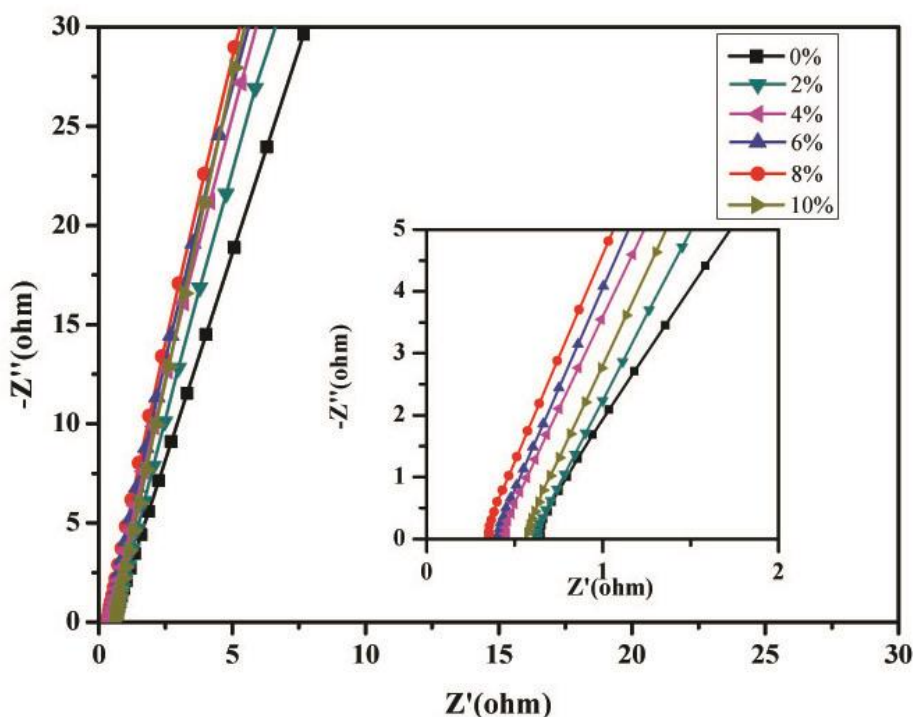


Figure 5. AC impedance spectra for PVA-KOH-HNTs ASPEs with different HNTs contents; the inset for high frequency region of spectra. ($m(\text{KOH}):m(\text{PVA})=1.5:1.5$; 30 °C)

Table 1. Conductivities of PVA-HNTs-KOH ASPEs with different HNTs contents

HNTs content	$R_b(\Omega)$	σ ($S \cdot cm^{-1}$)
0%	0.65	0.039
2%	0.63	0.041
4%	0.45	0.057
6%	0.42	0.061
8%	0.36	0.071
10%	0.57	0.044

($m(KOH):m(PVA)=1.5:1.5$; 30 °C)

As mentioned in Introduction section, the nanocomposite ASPE has been studied by some groups, and some good results and mechanisms has been achieved. For example, PVA-TiO₂-KOH-H₂O ASPEs with σ between 0.102 and 0.171 S·cm⁻¹ were prepared by Wu et al [14] and was applied in Zn-Ni battery with an average capacity density of 230mA·h·g⁻¹. The function of TiO₂ filler was to retard or inhibit the recrystallization of PVA polymer and to increase or retain the domain of amorphous phase and create more free volume. And the ion transport benefited from such local structural relaxation and segmental motions of the polymer. A more effective promotion was offered by the blending of the ZrO₂ in PVA ASPE and the highest σ was obtained by Yang et al [15]. It was found that the addition of nano-ZrO₂ fillers into the PVA polymer matrix could significantly improve the electrochemical properties of ASPE. The researchers thought that the ionic mobility might be increased by defects or free volume at interface between the ZrO₂ fillers and the PVA polymer matrix. Furthermore, the application of α -Al₂O₃ as addition in PVA ASPE was achieved by Mohamad et al [16], however, the σ was only about 10⁻⁷ S·cm⁻¹. The σ increased to 10⁻⁴ S·cm⁻¹ with the usage of propylene carbonate, and a local effective pathway for the transport of OH⁻ ion appeared and made the transport faster. More recently, based on blending tetraethoxysilane (a precursor of SiO₂ filler) and crosslinking through glutaraldehyde, the PVA-SiO₂ nanocomposite polymer membranes with remarkable electronic performance was achieved by Yang et al [17]. The σ was 0.035 S·cm⁻¹ with 10 wt% SiO₂ at ambient temperature. Alkaline direct methanol fuel cells (DMFCs) comprised of this nanocomposite ASPE were assembled and examined. The highest peak power density with 19.57 mW·cm⁻² was obtained. The SiO₂ nanoparticles acted as a solid plasticizer capable of enhancing the chemical and thermal properties, and improve the dimensional stability. And the many hydroxide groups on the SiO₂ filler surfaces greatly enhanced the KOH retaining ability.

The conductivity of PVA-KOH-HNTs ASPE originated from two ionic conductive mechanisms: the ions were transferred along the polymer molecular chain through the combination-dissociation process between ions and the polar groups of the polymer; another major conductive factor in the ASPE was the KOH/H₂O system providing more ion transfer tunnels as a result of the swelling structure and the ions migration increased at higher water content in such system. Such two mechanisms both depended on the crystalline-to-amorphous ratio, which was reduced by the doping of HNTs. The accumulation and crystallization of the polymer chain could be hindered by the nanotube [14], and then the crystallinity of polymer electrolyte system reduced accompanying the increase of the amorphous region and free volume. Therefore, more ions were transferred in the same time resulting

from the developing of the motility of polymer chain segments, and finally the conductivity improved. The inner structure model of PVA-KOH-HNTs ASPE is shown in Figure 6. The conductivity began to decrease when the content of HNTs exceeded 8 wt% perhaps because the excess HNTs could break the continuity of ionic conductive phase owing to the aggregation of HNTs with higher surface energy in the polymer matrix.

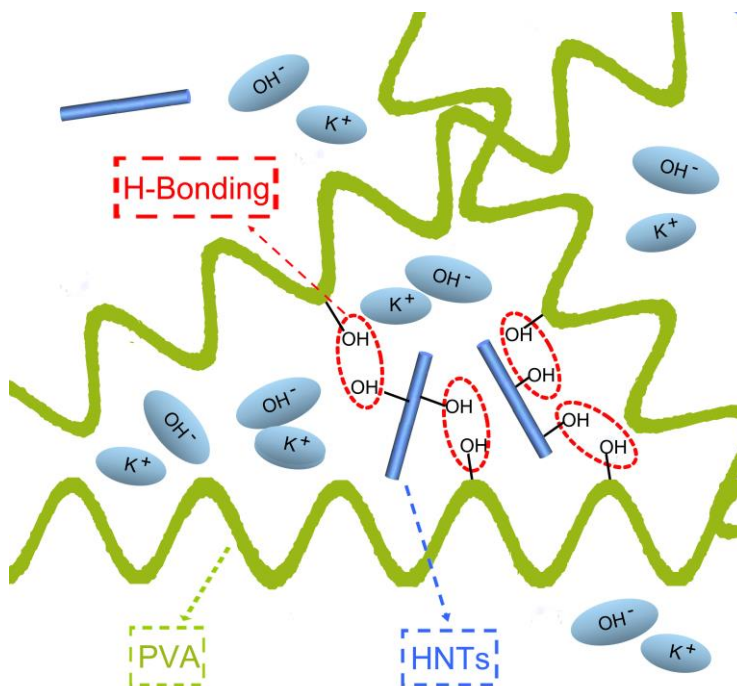


Figure 6. The illustration of the inner structure of PVA-KOH-HNTs ASPE

3.5 Influence of temperature on conductivity

The variation in AC impedance spectra of PVA-KOH-HNTs ASPEs ($m(\text{KOH}):m(\text{PVA})=1.5:1.5$; HNTs=8 wt%) in the temperature range 30~70 °C is depicted in Figure 7. Then, the R_b value was converted into the ionic conductivity value which was in the range of 0.071~0.087 $\text{S}\cdot\text{cm}^{-1}$ on the basis of the calculation, and it proved that ionic conductivity increased with the rise of temperature in the specified range. The improvement in conductivity with temperature could be attributed to hopping mechanism between coordinating sites and segmental motions of the polymer electrolytes [38]. As temperature increased, the amorphous ratio expanded and the structural relaxation of the polymer chains became more obvious. And the higher free volume and the vigorous segmental motion were provided resulting in the fast ion migration because the ions were easy to hop along the molecule chain. At the same time, the viscosity reduced with the increasing of temperature, whereas the diffusion ability of polymer matrix improved resulting in the promotion of the ion migration.

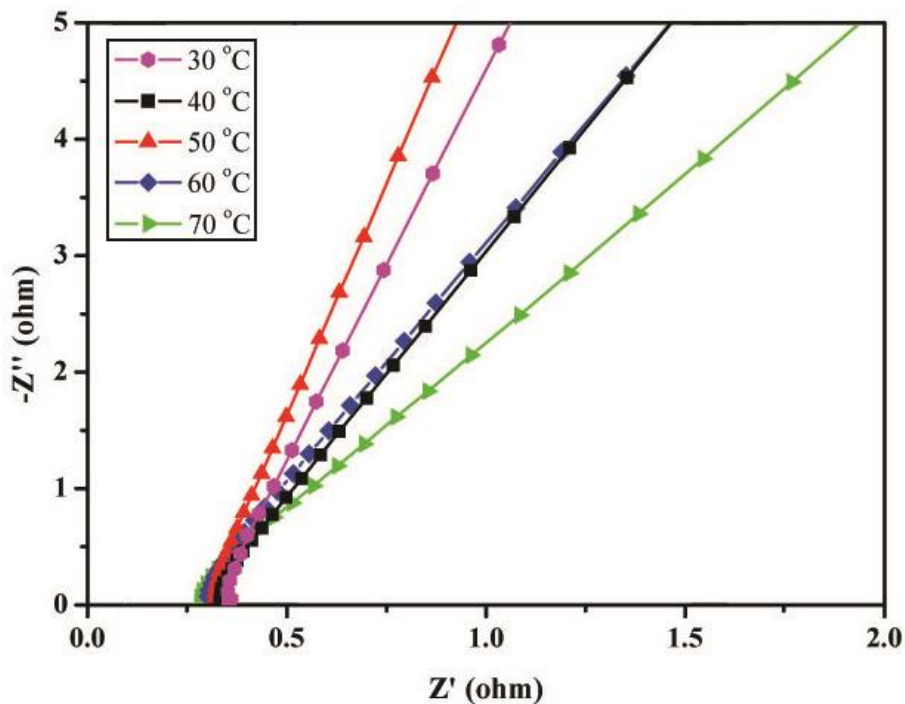


Figure 7. AC impedance spectra for PVA-KOH-HNTs ASPEs with temperature variation ($m(\text{KOH}):m(\text{PVA})=1.5:1.5$; HNTs=8 wt%)

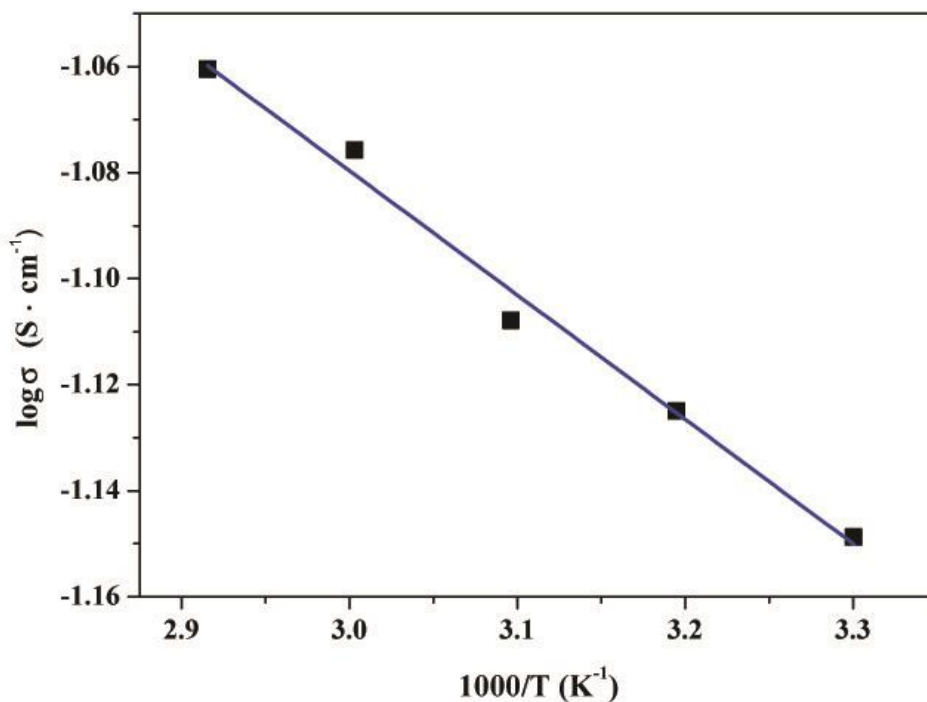


Figure 8. Arrhenius plot of conductivity for PVA-HNTs-KOH ASPE ($m(\text{KOH}):m(\text{PVA})=1.5:1.5$; HNTs content=8 wt%)

A distinct feature can be observed that the plot of $\log \sigma$ -versus- $1,000/T$ is almost linear in Figure 8 and obeys the equation 2, as predicted by Arrhenius activation equation [39].

$$\sigma = A \exp\left(\frac{-E_a}{RT}\right) \quad (\text{equation 2})$$

where A is the pre-exponential, E_a is the activation energy ($\text{kJ}\cdot\text{mol}^{-1}$), R is the universal gas constant $8.314 \text{ (J}\cdot\text{mol}^{-1}\cdot\text{K}^{-1})$, and T is the absolute temperature (K).

The E_a value of PVA-HNTs-KOH membrane was about $4.32 \text{ kJ}\cdot\text{mol}^{-1}$ which could be calculated from the Fig. 8 and equation 2. This value was lower than the PVA-KOH- H_2O membrane ($4.78 \text{ kJ}\cdot\text{mol}^{-1}$) [40], indicating that the energy barrier was lower accompanying easier ions migration [41]. The decrease of E_a with addition of HNTs was possibly due to the free volume increasing attributing to the increase of the amorphous phase and the flexibility of molecular chain [42].

3.6 Electrochemical stability

Electrochemical stability window was considered as one of the most important factors in practical applications of ASPE, and it was defined as a region of potential where no considerable Faradic current flowed through the electrolyte [43]. Cyclic voltammograms of the cell with the configuration of SS/PVA-HNTs-KOH/SS are shown in Figure 9. There's no significant difference in the electrochemical stability windows of the ASPEs. The electrochemical stability window was 1.43 V without HNTs and it increased to about 1.6 V after the addition of 8 wt\% HNTs. Outside this range, the reduction and oxidation of the polymer electrolyte and OH^- ions could take place.

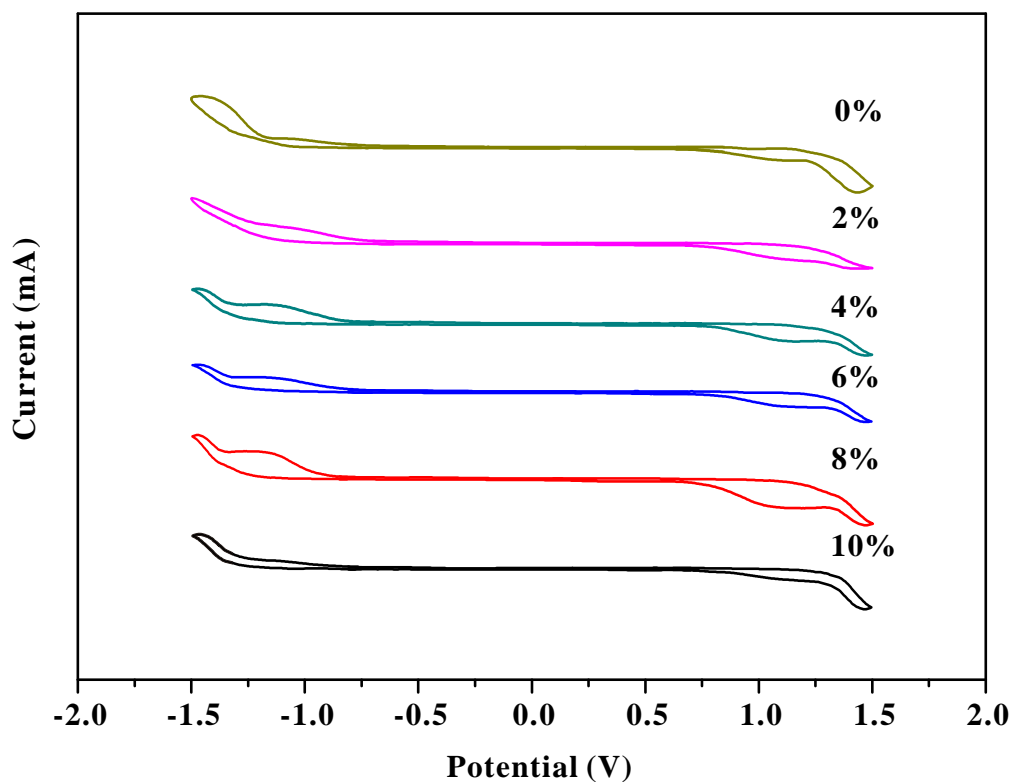


Figure 9. Cyclic voltammogram curves of the PVA-HNTs-KOH ASPEs with different HNTs contents ($m(\text{KOH}):m(\text{PVA})=1.5:1.5$; $30 \text{ }^\circ\text{C}$)

3.6 Thermal stability

Blending inorganic filler is an efficient method to enhance the thermal stability of the polymer. TGA curves of PVA-KOH-HNTs ASPEs with different HNTs contents are shown in Figure 10. For all samples, a large amount weight loss was observed below 150 °C corresponding to the loss of interstitial water held in the ASPE, where water molecules were linked by hydrogen bonds to the polar sites along the polymer chains. Besides, a two-step-degradation of ASPE without HNTs was exhibited, which showed two decomposition onset temperatures, T_{d1} and T_{d2} , at 174.6 °C and 435.3 °C, respectively. The PVA molecular chain broke into short chain at about 200 °C and degraded further into carbon char above 400 °C.

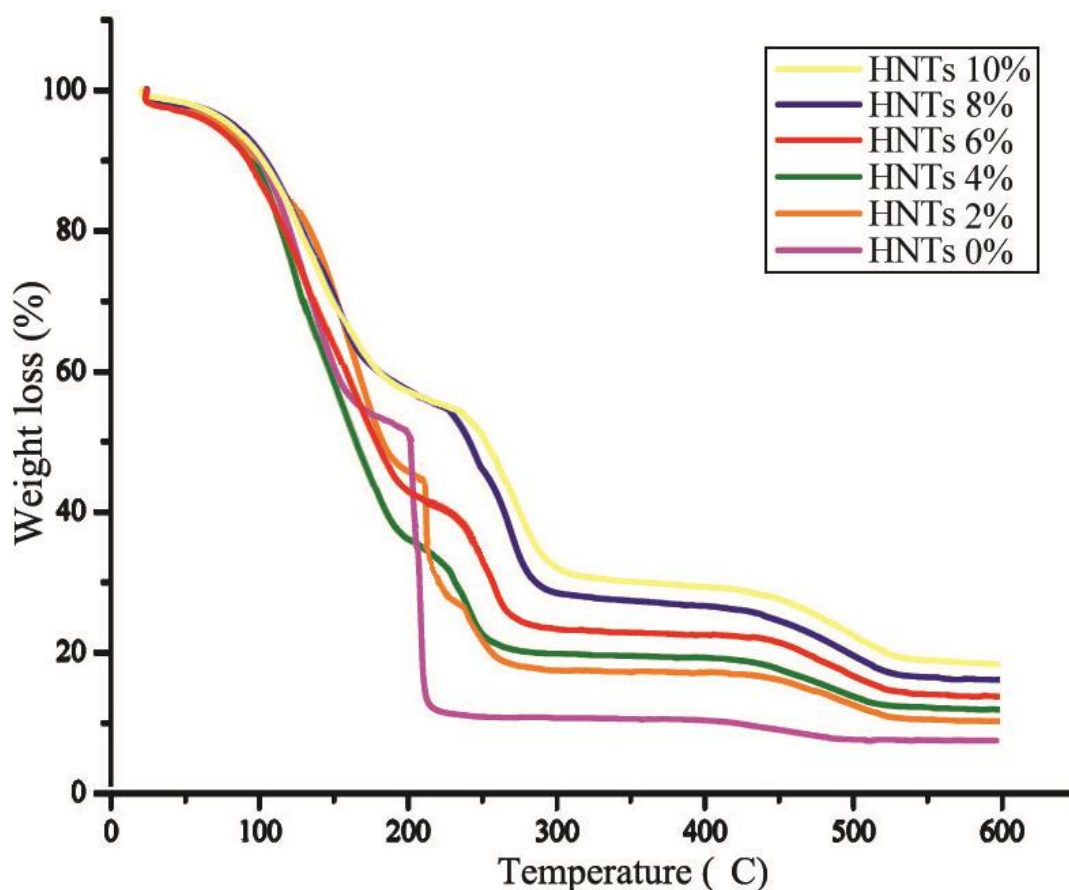


Figure 10. TGA thermograms for PVA-KOH-HNTs ASPEs with different HNTs contents ($m(\text{KOH}):m(\text{PVA})=1.5:1.5$)

In the entire degradation range from 150 °C to 600 °C, the higher thermal stability of the PVA-KOH-HNTs membranes with HNTs was observed compared with the membrane without HNTs. The variations in thermal stability of the PVA-HNTs membranes depended on the nanotubes contents. The polymer electrolytes with 2 wt%, 4 wt%, 6 wt%, 8 wt% and 10 wt% HNTs filler also showed two decomposition onset temperatures and the T_{d1} s were stable up to 192.7, 196.5, 203.2, 207.8 and 202.3 °C, respectively. What is more, the greater improvements were obtained in the T_{d2} s, which improved to 452.7, 457.4, 459.3, 462.2 and 460.9 °C. The addition of HNTs was significantly helpful to the

promotion of the ASPE thermal stability. On the one hand, the heat transmission was hindered by the addition of inorganic nano-filler and the degradation speed decreased; on the other hand, the volatilization of the thermal degradation products was obstructed.

3.7 Performance in Ni-MH battery of PVA-HNTs-KOH ASPE

As described above, the PVA-HNTs-KOH ASPE possessed high ionic conductivity and electrochemical stability. So it was expected that this electrolyte could be a potential candidate for Ni-MH battery. Ni-MH battery comprising of PVA-HNTs-KOH ($m(\text{PVA}):m(\text{KOH})=1.5:1.5$; HNTs=8 wt%.) ASPE, $\text{Ni}(\text{OH})_2/\text{NiOOH}$ as positive electrode and hydrogen storage alloy powder as negative electrode have been assembled and subjected to charge-discharge studies.

The electrochemical properties were detected by galvanostatic charge/discharge. The result in Figure 11 shows that for the PVA-HNTs-KOH ASPE Ni-MH battery, the first-cycle discharge capacity was $143 \text{ mAh}\cdot\text{g}^{-1}$, then it gradually improved to about $223 \text{ mAh}\cdot\text{g}^{-1}$ and stabilized around $215 \text{ mAh}\cdot\text{g}^{-1}$ following the activation in the initial several cycles. This phenomenon perhaps was a result of the improvement of the compatibility between the ASPE membrane and electrode surface after initial charge/discharge cycles and the electrode reaction was promoted. However, it reduced after 8 cycles because of the corrosion of the hydrogen storage alloy, and the surface of the negative electrode became green.

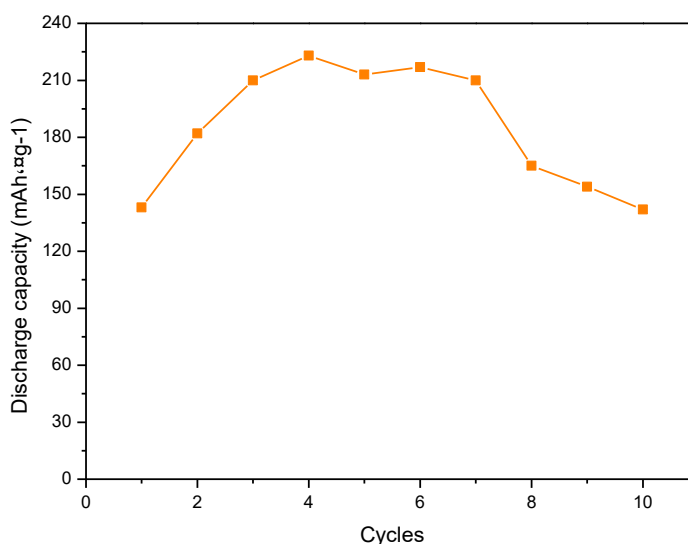


Figure 11. Discharge capacity of the assembled Ni-MH battery with PVA-HNTs-KOH ASPE

4. CONCLUSION

PVA and KOH have been used to prepare ASPE membranes with HNTs as filler. Compared to the PVA-KOH ASPE, the ionic conductivity of PVA-KOH-HNTs ASPE increased to $0.071 \text{ S}\cdot\text{cm}^{-1}$ at $30 \text{ }^\circ\text{C}$, and the value increased with the temperature rise. The ion transport activation energy derived

from the slopes of the Arrhenius plots decreased to $4.32 \text{ kJ}\cdot\text{mol}^{-1}$. In addition, the thermal stability could be improved by the doping of the HNTs. The Ni-MH battery was assembled using PVA-KOH-HNTs ASPE and the highest discharge capacity of $223 \text{ mAh}\cdot\text{g}^{-1}$ was obtained.

ACKNOWLEDGEMENTS

This work was supported by National Natural Science Foundation of China (51403056), International Science and Technology Cooperation Projects of He'nan Province (144300510041). This work was also supported by Doctoral Fund of Henan Polytechnic University (B2012-052).

References

1. J. Cheng, G. Q. Yang, K. B. Zhang, G. H. He, J. Jia, H. M. Yu, F. Y. Gai, L. D. Li, C. Hao and F. X. Zhang, *J. Membrane Sci.* 501 (2016) 100.
2. T. C. Zhou, R. Shao, S. Chen, X. M. He, J. L. Qiao and J. J. Zhang, *J. Power Sources* 293 (2015) 946.
3. G. W. Li, Y. Wang, J. Pan, J. J. Han, Q. Liu, X. Q. Li, P. C. Li, C. Chen, L. Xiao, J. T. Lu and L. Zhuang, *Int. J. Hydrogen Energ.* 40 (2015) 6655.
4. J. M. Yang, N. C. Wang and H. C. Chiu, *J. Membrane Sci.* 457 (2014) 139.
5. F. F. Song, Y. S. Fu, Y. Gao, J. D. Li, J. L. Qiao, X. D. Zhou and Y. Y. Liu., *Electrochim. Acta* 177 (2015) 137.
6. A. B. Yuan and J. Zhao, *Electrochim. Acta* 51 (2006) 2452.
7. Y. Gao, F. F. Song, J. L. Qiao, S. L. Chen, X. X. Zhao and J. J. Zhang, *Electrochim. Acta* 177 (2015) 201.
8. Z. Zhang, C. C. Zuo, Z. H. Liu, Y. Yu, Y. X. Zuo and Y. Song, *J. Power Sources* 251 (2014) 470.
9. C. C. Yang, S. J. Lin and S. T. Hsu, *J. Power Sources* 122 (2003) 210.
10. J. M. Yang, N. C. Wang and H. C. Chiu, *J. Membrane Sci.* 457 (2014) 139.
11. T. C. Zhou, R. Shao, S. Chen, X. M. He, J. L. Qiao and J. J. Zhang, *J. Power Sources* 293 (2015) 946.
12. Y. Gao, F. F. Song, J. L. Qiao, S. L. Chen, X. X. Zhao and J. J. Zhang, *Electrochim. Acta* 177 (2015) 201.
13. C. C. Yang, S. J. Lin and S. T. Hsu, *J. Power Sources* 122 (2003) 210.
14. Q. M. Wu, J. F. Zhang and S. B. Sang, *J. Phys. Chem. Solids* 69 (2008) 2691.
15. C. C. Yang, *Mater. Sci. Eng., B* 131 (2006) 256.
16. A. A. Mohamad and A. K. Arof, *Mater. Lett.* 61 (2007) 3096.
17. C. C. Yang, Y. J. Li and T. H. Liou, *Desalination* 276 (2011) 366.
18. S. H. Sang, J. F. Zhang, Q. M. Wu and Y. G. Liao, *Electrochim. Acta* 52 (2007) 7315.
19. C. C. Yang and S. J. Lin, *J. Power Sources* 112 (2002) 497.
20. Y. Lvov, W. Wang, L. Zhang and R. Fakhrullin, *Adv. Mater.* 28 (2016) 1227.
21. M. Massaroa, R. Amaratib, G. Cavallaroc, S. Guernellib, G. Lazzarac, S. Miliotoc, R. Notoa, P. Pomad and S. Rielaa, *Colloid Surface B* 140 (2016) 505.
22. F. Cravero and G. J. Churchman, *Clay Miner.* 51 (2016) 417.
23. Q. Peng, M. X. Liu, J. W. Zheng and C. G. Zhou, *Micropor. Mesopro. Mat.* 201 (2015) 190.
24. Y. Jin, R. Yendluri, B. Chen, J. B. Wang and Y. Lvov, *J. Colloid Interface Sci.* 466 (2016) 254.
25. H. Afshar and A. Ghaee, *Carbohydr. Polym.* 151 (2016) 1120.
26. Y. Zhang, A. D. Tang, H. M. Yang and J. Ouyang. *Clay Sci.* 119 (2016) 8.
27. Y. N. Peng, D. Y. Tan and A. B. Fa'iza, *Appl. Clay Sci.* 112-113 (2015) 75.
28. X. Y. Wan, Y. Q. Zhan, G. Y. Zeng and Y. He. *Appl. Surf. Sci.* 393 (2017) 1.
29. C. Chiu, *Compos. Part B- Eng.* 110 (2017) 193.

30. E. Oliaei and B. Kaffashi, *Polymer* 104 (2016) 104.
31. K. N. Shilpa, K. S. Nithin, S. Sachhidanand, B. S. Madhukar and Siddaramaiah, *J. Alloys Compd.* 694 (2017) 884.
32. Y. L. Luo, Q. B. Wei, F. Xu, Y. S. Chen, L. H. Fan and C. H. Zhang, *Mater. Chem. Phys.* 118 (2009) 329.
33. H. X. Yu, Y. T. Zhang, X. B. Sun, J. D. Liu and H. Q. Zhang, *Chem. Eng. J.* 237 (2014) 322.
34. S. J. Lue, J. Y. Chen and J. M. Yang, *J. Macromol. Sci. B* 47 (2008), 39.
35. M. L. Du, B. C. Guo and D. M. Jia, *Eur. Polym. J.* 42 (2006) 1362.
36. J. Suk, Y. H. Lee, D. Y. Kim, D. W. Kim, S. Y. Cho, J. M. Kim and Y. Kang, *J. Power Sources* 334 (2016) 154.
37. A. L. Wang, H. Xu, Q. Zhou, X. Liu, Z. Y. Li, R. Gao, N. Wu, Y. G. Guo, H. Y. Li and L. Y. Zhang, *Electrochim. Acta* 212 (2016) 372.
38. K. P. Radha, S. Selvasekarapandian, S. Karthikeyan, M. Hema and C. Sanjeeviraja, *Ionics* 19 (2013) 1437.
39. W. Y. Li, L. Chen, Y. H. Sun, C. X. Wang, Y. G. Wang and Y. Y. Xia, *Solid State Ionics* 300 (2017) 114.
40. C. C. Yang, *Mater. Lett.* 58 (2004) 33.
41. B. B. Li, X. Lu, J. G. Yuan, Y. F. Zhu and L. Q. Zhu, *Ionics* 21 (2015) 141.
42. H. L. Huang, X. G. Ma, R. Wang, L. Zhang and Z. H. Deng, *Solid State Ionics* 267 (2014) 54.
43. G. A. Tiruye, D. Muñoz-Torrero, J. Palma, M. Anderson and R. Marcilla, *J. Power Sources* 279 (2015) 472.

© 2017 The Authors. Published by ESG (www.electrochemsci.org). This article is an open access article distributed under the terms and conditions of the Creative Commons Attribution license (<http://creativecommons.org/licenses/by/4.0/>).